O_2 (molecular). It is thus possible that CO_2 will finally dissociate into its constituent elements, at multimegabar pressures, directly from the α-quartz phase.

The stability of the α-quartz structure over such a large pressure range is surprising, particularly when compared with SiO_2, where α-quartz is observed to transform into coesite at 2.1 GPa and then into stishovite at 7.6 GPa. We suggest that CO_2 behaves differently because the C sp^3 hybrid is energetically closer than the Si sp^3 hybrid to the p state of the bridging oxygen. Structurally, this implies stabilization of a more covalent C–O–C bond and, more specifically, a decrease of the C–O–C bending angle with respect to Si–O–Si. This is consistent with our observation that the C–O–C bending angle in all fourfold coordinated CO_2 structures is systematically lower than the corresponding values for SiO_2 (for α-quartz at zero pressure, we find for CO_2 a bending angle of 137°, compared with a value of 144° for SiO_2). Preference for low C–O–C bending angles may then explain why CO_2 cristobalite, where all bending angles are fixed by symmetry to 180°, and coesite, where the same is true for one of the bending angles, are energetically disfavored (Fig. 2). This may also be the rationale for the appearance of the layered-CO_2 structure, and m-chalcopyrite, where the bending angles are found to be about 109° at all pressures.

If α-quartz CO_2 could be quenched to zero pressure, we predict that its lattice parameters would be $a = 4.13$ Å and $c = 4.58$ Å, its density 3.28 g/cm^3, and its bulk modulus 183 GPa. It would be insulating, with an energy gap that we estimate to be around 10 eV (*18*). We also calculated the piezoelectric strain coefficient (*19*) of α-quartz CO_2 at zero pressure, and found it to be 1.0 pC/N, about 40% that of SiO_2, possibly as a result of the lower ionicity of α-quartz CO_2. Finally, we give an estimate of the relative value of the second harmonic intensity I_{SH} of α-quartz CO_2 with respect to that of α-quartz SiO_2. I_{SH} is proportional (*20*) to the square of the second-order susceptibility $\chi^{(2)}$ that can be estimated with Miller's rule (*21*), and the fact that first-order susceptibility roughly scales linearly with electron density and with the inverse square of the energy gap. I_{SH} of α-quartz CO_2 estimated in this way is about 50 times larger than that of α-quartz SiO_2.

Note added in proof: Recently, Iota *et al.* (*22*) have shown that, in agreement with our findings, quartzlike CO_2 can in fact be synthesized above 40 GPa and 1800 K.

References and Notes

1. C. A. English and J. A. Venables, *Proc. R. Soc. London Ser. A.* **340**, 57 (1974).
2. B. Kuchta and R. D. Etters, *Phys. Rev. B* **38**, 6265 (1988).
3. D. A. Dows and V. Schettino, *J. Chem. Phys.* **58**, 5009 (1973).
4. H. Olijnyk *et al.*, *ibid.* **88**, 4204 (1988).
5. K. Aoki *et al.*, *Science* **263**, 356 (1994).
6. F. Gygi, *Comput. Mater. Sci.* **10**, 63 (1998).
7. R. Lu and A. M. Hofmeister, *Phys. Rev. B* **52**, 3985 (1995).
8. H. Olijnyk and A. P. Jephcoat, *ibid.* **57**, 879 (1998).
9. L. Liu, *Earth Planet. Sci. Lett.* **71**, 104 (1984).
10. P. Focher *et al.*, *Europhys. Lett.* **36**, 345 (1994).
11. S. Scandolo *et al.*, *Phys. Rev. Lett.* **74**, 4015 (1995); M. Bernasconi *et al.*, *ibid.* **78**, 2008 (1997); J. Kohanoff *et al.*, *ibid.*, p. 2783; F. Ancilotto *et al.*, *Science* **275**, 1288 (1997); S. Serra *et al.*, *Phys. Rev. Lett.* **80**, 5160 (1998); C. Cavazzoni *et al.*, *Science* **283**, 44 (1999).
12. S. Bernard *et al.*, *Phys. Rev. Lett.* **81**, 2092 (1998).
13. A. D. Becke, *Phys. Rev. A* **38**, 3098 (1988); C. Lee, W. Yang, R. G. Parr, *ibid. B* **37**, 785 (1988).
14. L. Kleinman and D. M. Bylander, *Phys. Rev. Lett.* **48**, 1425 (1982).
15. N. Trouiller and J. L. Martins, *Phys. Rev. B* **43**, 1993 (1991).
16. S. Nosé, *Mol. Phys.* **52**, 255 (1984).
17. In this structure carbon is fourfold coordinated to oxygen, oxygen twofold coordinated to carbon, and the C–O–C bending angle is 109°.
18. The LDA is known to underestimate band gaps. We calculate a LDA/GGA gap of 6.5 eV for α-quartz CO_2. In α-quartz SiO_2 the LDA/GGA band gap is also 6.5 eV, compared with an experimental value of about 10 eV. Here we assume that the same correction applies to CO_2.
19. D. Vanderbilt, available at xxx.lanl.gov/abs/cond-mat/9903137.
20. Y. R. Shen, *The Principles of Nonlinear Optics* (Wiley, New York, 1984).
21. R. C. Miller, *Appl. Phys. Lett.* **5**, 17 (1964); Y. R. Shen, in (*20*), p. 37.
22. V. Iota, C. S. Yoo, H. Cynn, *Science* **283**, 1510 (1999).

23. We acknowledge partial support from INFM and MURST.

21 December 1998; accepted 18 March 1999

Global Distribution of Crustal Magnetization Discovered by the Mars Global Surveyor MAG/ER Experiment

M. H. Acuña,[1] J. E. P. Connerney,[1] N. F. Ness,[2] R. P. Lin,[3] D. Mitchell,[3] C. W. Carlson,[3] J. McFadden,[3] K. A. Anderson,[3] H. Rème,[4] C. Mazelle,[4] D. Vignes,[4] P. Wasilewski,[1] P. Cloutier[5]

Vector magnetic field observations of the martian crust were acquired by the Mars Global Surveyor (MGS) magnetic field experiment/electron reflectometer (MAG/ER) during the aerobraking and science phasing orbits, at altitudes between ~100 and 200 kilometers. Magnetic field sources of multiple scales, strength, and geometry were observed. There is a correlation between the location of the sources and the ancient cratered terrain of the martian highlands. The absence of crustal magnetism near large impact basins such as Hellas and Argyre implies cessation of internal dynamo action during the early Naochian epoch (~4 billion years ago). Sources with equivalent magnetic moments as large as 1.3 × 10^{17} ampere-meter^2 in the Terra Sirenum region contribute to the development of an asymmetrical, time-variable obstacle to solar wind flow around Mars.

The primary science goals of the MAG/ER investigation are the detection and characterization of the magnetic field of the planet and the study of its interaction with the solar wind. Vector measurements of the ambient magnetic field are acquired by a twin fluxgate magnetometer system. An electron reflection analyzer is used to remotely sense magnetic fields of planetary origin at the top of the martian atmosphere and to provide information about the local electron distribution function (*1*, *2*). Measurements made early in the mission established unambiguously that Mars does not currently possess a significant global magnetic field, with an estimated upper limit for a Mars dipole moment of ~2 × 10^{18} A-m^2.

At the same time the detection of strong, small-scale crustal magnetic sources associated with the ancient, heavily cratered terrain revealed that Mars must have had an internal active dynamo in its past, which is now extinct (*1*).

The first part of the aerobraking phase of MGS (AB1) was carried out between September and November 1997 and was followed by aerobraking hiatus orbits (AHO) and science phasing orbits SPO1 and SPO2 from March to July 1998. The latter were designed to allow the heliocentric motion of Mars to bring the spacecraft orbit plane into the desired alignment with the Mars-sun direction before initiating the second aerobraking phase AB2 and "pop-up" maneuver which would raise periapsis to achieve the final mapping orbit. These recently com-

[1]NASA Goddard Space Flight Center, Greenbelt, MD 20771, USA. [2]Bartol Research Institute, University of Delaware, Newark, DE 19716, USA. [3]Space Sciences Laboratory, University of California, Berkeley, CA 94720, USA. [4]Centre d'Etude Spatiale des Rayonnements, 31028 Toulouse Cedex 4, France. [5]Department of Space Physics and Astronomy, Rice University, Houston, TX, 77005, USA.

pleted maneuvers circularized the orbit at ~380-km altitude in the 2 a.m.–2 p.m. local time plane. During AB1, AHO, SPO1, and SPO2 the latitude of periapsis, starting around ~30°N, progressed slowly toward and over the north pole, allowing detailed sampling of this region at altitudes between 170 and 200 km. The AB2 phase started in late December 1998 lowered periapsis altitude to ~100 km and introduced rapid southward progression of periapsis latitude, reaching a maximum of 87°S before the termination of aerobraking. Magnetic field measurements were performed during most of AB2 for periods of 30 to 60 min centered around periapsis.

The instrumentation associated with the MAG/ER investigation has been described in more detail in (*1*) and (*2*) and a brief summary is given in (*3*). Using data compression, the fluxgate magnetometers are capable of acquiring up to 32 vector samples per second when downlink rates are high, but here we report results obtained with "full word" 12-bit vector samples that occurred every 0.75 to 3 s depending on the selected data rate. This sampling rate was sufficient for the unaliased detection of crustal magnetic sources at altitudes >100 km and a spacecraft velocity at periapsis of ~4 km s^{-1}. The estimated accuracy of the measurements is ±3 nT (*4*). We report here observations carried out during the 916 elliptical orbits for which magnetic field data were acquired, from the start to the end of AB1, through AHO, SPO1, and SPO2, and to near the end of AB2 when spacecraft resource limitations could no longer support data acquisition. Longitude coverage was globally distributed but sparse. Considering that the equivalent "pixel" size of the magnetic field observations can be represented as a square with a side dimension about equivalent to the orbital height, the spatial coverage achieved below 200 km amounts to ~20% of the surface of the planet.

The dense spatial coverage achieved by the MGS orbit over the north pole of Mars made possible the detailed mapping of several relatively weak but discrete magnetic source regions centered around 330°W longitude and extending from 60°N to almost 90°N in latitude (Fig. 1). The highly elliptical orbit of MGS with varying periapsis altitude introduced complications in the modeling and estimation of possible source geometry and strength (magnetic moment). As the spacecraft altitude increased, the shorter spatial wavelengths associated with the crustal sources were attenuated. Magnetic profiles obtained on adjacent passes (nearby in longitude), when plotted as a function of time, may appear different if the altitude was variable. The MGS observations over the north pole of Mars were acquired over periapsis altitudes between 170 and 200 km, which results in negligible variation in magnetic profiles of the sources over adjacent orbits. An additional source of error is the contribution of "magnetic noise" by ionospheric currents induced by the Mars–solar wind interaction, which becomes important above 120 to 150 km. The reduction of source geometry and strength to a common altitude using continuation methods similar to those used for terrestrial magnetic anomalies (*5*) has not been carried out. Because the draping of the interplanetary

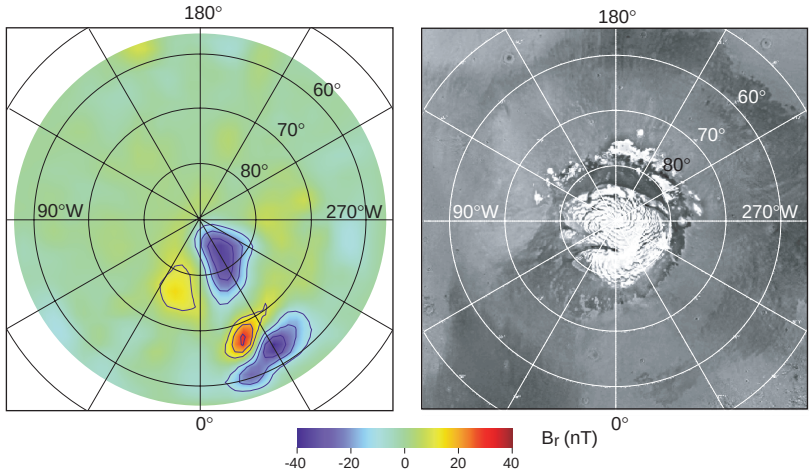

Fig. 1. Polar stereographic projection from 55°N latitude to the north pole of Mars. (**Left**) Radial (vertical) component of the field, where blue represents the magnetic field direction into the planet and red represents the direction out of the planet. The spacecraft periapsis altitude was ~170 km during this time. Data taken between 170 and 200 km have been organized in 100 km by 100 km bins, median sorted, and smoothed to yield the contours shown. (**Right**) Mars north polar region image of topography corresponding to the left panel above included for reference (*16*). The north polar ice cap of Mars is the white, scalloped region visible in the center of the figure and is elevated above its surroundings by ~3 km.

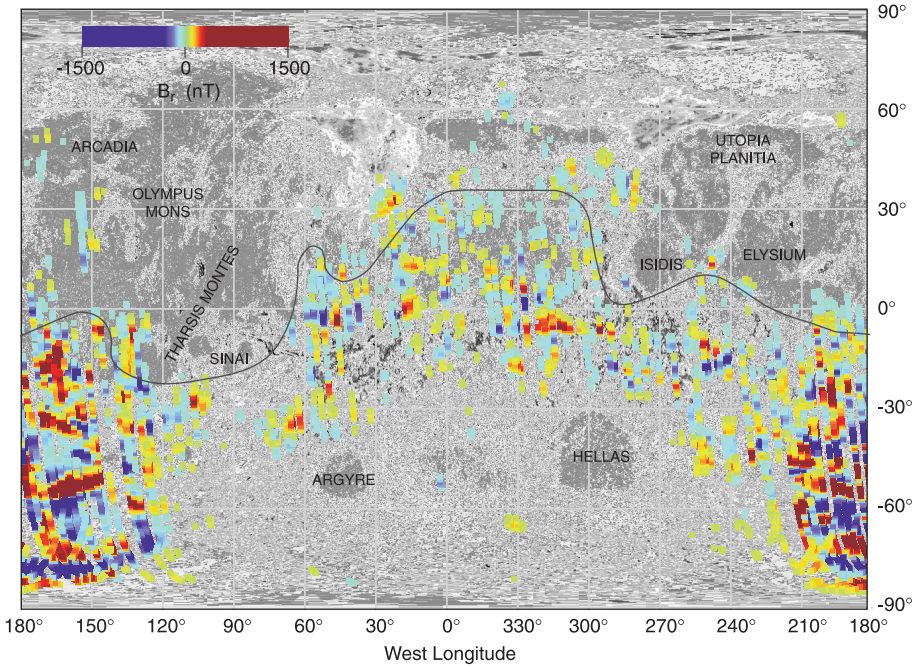

Fig. 2. Map showing the location and intensity of crustal magnetic sources detected by the MGS-MAG/ER experiment superimposed on a topographic image of Mars (*16*). The measured radial (vertical) component of the magnetic field associated with the crustal sources is illustrated by the color scale shown. No correction has been made for the varying spacecraft altitude, which results in attenuation of the small-scale signature of the sources with increasing altitude. The dichotomy boundary is marked by the solid line separating the northern lowlands from the southern highlands (*8*). Data acquired at altitudes between ~100 and 200 km for 916 elliptical orbits are included. The color scale has been chosen to illustrate the relative intensity of the crustal sources. Note the large range in magnetic field intensity associated with this color scale versus that shown in Fig. 1.

magnetic field over the martian ionosphere due to the solar wind interaction results in mostly horizontal components parallel to the planet's surface (*6*), the radial component of the crustal field is largely free of ionospheric contributions and may be used as a sensitive indicator of the presence of magnetic sources in the crust.

The data from the north polar region where MGS coverage was dense were binned and sorted into 100 km by 100 km regions and the median value of the bins determined. This procedure yielded smoothed isocontours of the radial component of the crustal magnetic field which range from −40 nT to +40 nT at 170 to 200 km (Fig. 1). This process yielded estimated uncertainties ranging from ~3 to 10 nT, depending on the number of estimates in each bin, resulting in smaller uncertainties at higher latitudes. An approximate calculation using a single-dipole model at ~100-km depth yields an equivalent moment of $\sim 10^{16}$ A-m^2 for these sources. There were no other crustal magnetic sources in this region of the northern lowlands, which is one of the youngest geological provinces of Mars as determined by the low impact crater density and evidence of repeated volcanism. No gravity, topography, or geological feature has been associated with the north polar magnetic sources detected by MGS although the presence in this region of significant gravity anomalies is suggestive (*7*) of an association with deep, iron-rich concentrations in the crust.

The Mars–solar wind interaction is primarily atmospheric in nature (*1*), and the pronounced draping of the interplanetary magnetic field over the ionosphere in the north polar region, superposed with the magnetic field from the crustal sources, gives rise to asymmetries and the formation of localized Earth-like "cusps" and/or magnetic reconnection regions where plasmas from the martian ionosphere, its comet-like tail, and the solar wind can intermix.

Contrary to the observations in SPO1 and SPO2, as the latitude of periapsis progressed southward in the AB2 phase (in 3 weeks), more frequent and intense crustal sources were detected, particularly in the range of 120°W to 210°W and 30°S to 85°S, where total fields as large as ~1600 nT at orbital altitude (~100 km) were observed (radial component shown in Figs. 2 to 4). Because of the sparse coverage over these regions, it was not possible to bin and median sort the data. Superposition of data obtained for multiple nonoverlapping orbits over the planet's surface was used to identify and map the distribution of magnetic sources in the martian crust. The wide dynamic range in the strength (magnetic moment) of the sources makes their graphic visualization difficult with linear color scales on a global map (Fig. 2), although this map helps to illustrate the relative location and intensity of the sources. The weaker magnetic sources disappear in the background, overwhelmed by more intense sources. In order to approximate a logarithmic representation of field magnitude, the color scale was adjusted to make all the sources look similar using a highly compressed color scale. Information about their relative intensity is lost, but the location and approximate morphology of all the sources detected were enhanced (Figs. 3 and 4). The majority of the crustal magnetic sources lie south of the dichotomy boundary on the

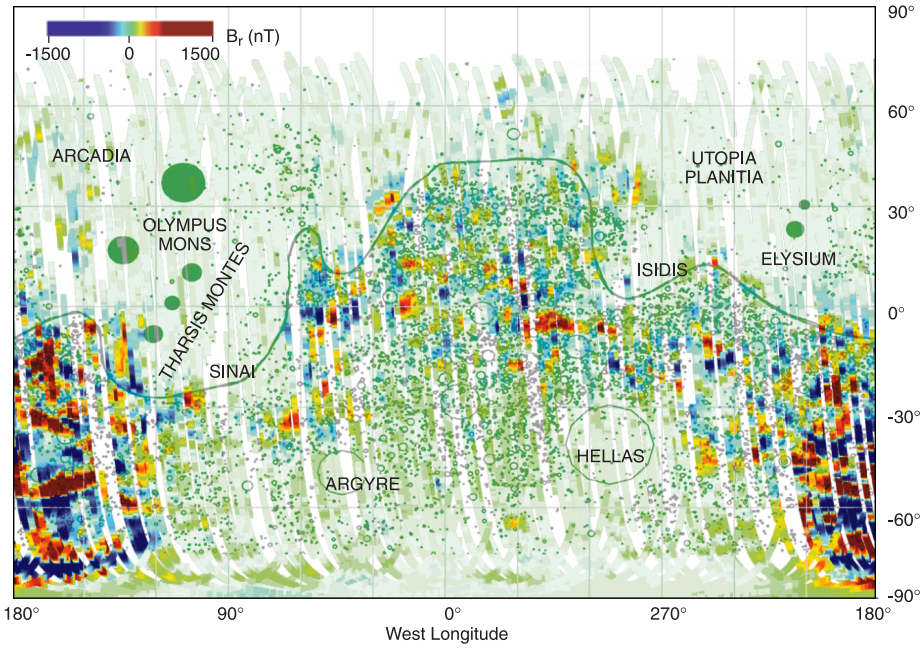

Fig. 3. Map showing the distribution of crustal magnetic field sources superimposed on a map showing the distribution of craters greater than 15 km in diameter (*8*) and the dichotomy boundary (solid line). The spacecraft tracks below 200-km altitude have been projected onto the surface as light green thick lines to illustrate the orbital coverage. The thickness of the subsatellite tracks has been chosen to approximate the equivalent "pixel" size for the observations as discussed in the text. The measured radial (vertical) component of the magnetic field associated with the crustal sources is illustrated using a color scale that reveals the location of significant magnetic sources detected regardless of intensity. Note the high correlation between the region where magnetic crustal sources appear and high crater densities (ancient terrain) and the absence of magnetic imprints within the Hellas, Argyre, and Isidis impact basins. No magnetic signatures have been found over Elysium, Olympus Mons, or Tharsis Montes.

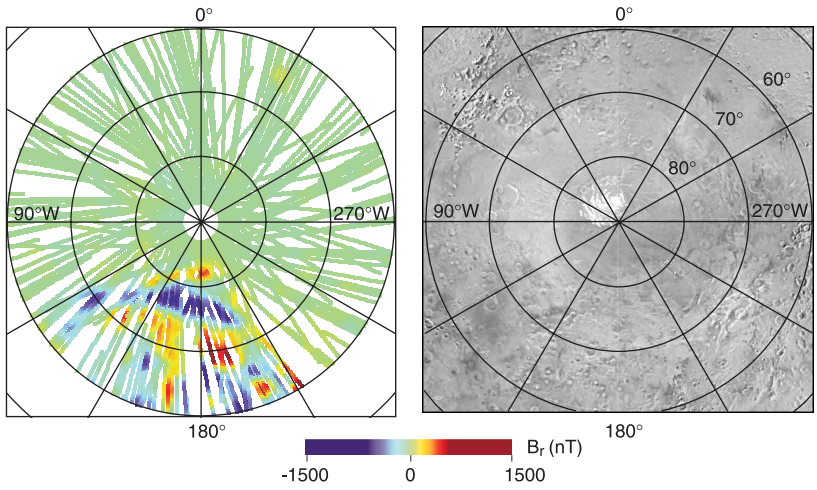

Fig. 4. Polar stereographic projection from 55°S to the south pole of Mars. (**Left**) The radial (vertical) component of the magnetic field is illustrated using the same color scale as Fig. 3. Coverage of this region is sparse and does not allow binning, sorting, and smoothing as done for Fig 1. Superposition of magnetic field data acquired from largely nonoverlapping orbits is shown instead. Note the change in intensity scale with respect to Fig. 1. The polar stereographic projection provides a more realistic spatial illustration of the Terra Sirenum crustal sources, where linearly structured magnetic field sources are found. (**Right**) Mars south polar region topographic image corresponding to the left panel above included for reference (*16*).

ancient, densely cratered terrain of the highlands and extend ~60° south of this boundary (Fig. 3). The crustal dichotomy is the geologic division between the heavily cratered highlands to the south and the relatively young, smooth plains to the north where the crust is thinner (*5*). There is an apparent correlation between the location of the sources and the impact crater densities (*8*) in this region caused primarily by the modification of the ancient crust over impact basins, but no association between individual craters and magnetic sources has been found. No magnetic sources were detected over Tharsis, Elysium, Valles Marineris, or any of the other major martian volcanic edifices. The large impacts that formed the Hellas and Argyre basins and that are believed to have formed in the early Naochian epoch [~4 billion years ago (Ga)], are also not associated with magnetic sources (Fig. 3). The absence of crustal magnetism in these basins and their surroundings implies that the Mars dynamo had already ceased to operate when these impact basins were formed, about 3.9 Ga. This evidence supports the models of a hot early Mars immediately after accretion (~4.5 Ga), followed by rapid cooling and crust formation (*9*, *10*). The dynamo operated perhaps for a few hundred million years after accretion before shutting off, and the ancient, iron-rich crust formed and cooled below the Curie point (*11*) during this time. The formation of the dichotomy boundary postdates the cessation of dynamo action because of the clear magnetic differentiation between the terrains on either side of the boundary. There was no magnetization of the crust north of the dichotomy boundary in spite of active volcanism and magmatic flows because dynamo action had ceased. Crustal magnetization can also be destroyed by reheating or reworking of the crust without altering its composition. The southernmost limit of the crustal magnetization region appears to be associated with the destruction or modification of the magnetized crust by the impacts that created the Argyre and Hellas basins. For the Hellas basin, a discontinuous, outer ring of magnetization was observed to the northwest and east of the basin in the global distribution maps, perhaps indicating the maximum extent of alteration of the crust by the impact. In the north, the impact that formed the Isidis basin also left a clear imprint that is reflected in the shape of the dichotomy boundary in this region and the absence of magnetic crustal sources within the basin. This evidence shows that any processes that took place after the cessation of dynamo action only modified the ancient, magnetized, thin crust through deep impacts, magmatic flows, tectonics, or reheating above the Curie point. The MGS magnetic field data therefore are consistent with a model in which the dichotomy boundary is formed by the combined effects of large impacts, induced volcanism, magmatic flows, and widespread tectonism (*12*).

These results place constraints on current models of Mars interior and thermal evolution and the assumed sulfur content by weight of the core. This is a critical parameter in theoretical models of interior evolution (differentiation into a crust, mantle, and core) that determines how fast and if a solid core forms (*10*). The martian meteorites do not exhibit magnetic properties that are consistent with the magnetization required to explain the strength of the crustal sources (*1*) and hence may not constitute reliable indicators of the early interior composition or intensity of the martian paleofield. Our results also imply that the martian dynamo may not have played a significant role in controlling the loss of volatiles from Mars because of its short life time, supporting calculations of the rate of loss of oxygen ions (or water loss) due to ion pick-up by the solar wind that assume the absence of a magnetic field since the time of planetary accretion (*1*, *13*).

The most intense magnetic crustal sources detected by MGS-MAG/ER lie in the Terra Sirenum region (120°W to 210°W; 30°S to 85°S) where measured total field intensities at ~100-km altitude exceeded 1500 nT (Figs. 3 and 4). The estimated total net magnetic moment of this region was computed using the measurements acquired in the circular orbit at 400-km altitude and amounts to $\sim 1.3 \times 10^{17}$ A-m^2. This moment is sufficiently high such that the resulting magnetic fields in and above the ionosphere locally increase the total pressure (thermal plus magnetic) that stands off and deflects the solar wind at Mars, resulting in an asymmetric bow shock when this region rotates through the sunlit side of the planet. This configuration also results in the formation of extended, multiple, Earth-like magnetospheric "cusps" and magnetic reconnection regions with the interplanetary magnetic field, similar to those formed over the north polar crustal sources discussed earlier. Connerney *et al.* (*14*) present analytical models of the extended sources in the Terra Sirenum region and their implications. The MGS-MAG/ER results also refine interpretations of data obtained by previous Mars missions and the long standing debate over the existence of a planetary magnetic field. Phobos 2 investigators speculated on the possible existence of a field noting 8-, 12- and 24-hour periodicities in spectral analyses of magnetic field data taken along the orbit of Phobos 2 (*15*). On the basis of the MGS-MAG/ER observations, we conclude that the Terra Sirenum crustal magnetic sources may have been responsible for the observed periodicities in the measured field. The 24-hour period corresponds to Mars' rotation rate, while the 8- and 12-hour periodicities arise as a result of the commensurability between the martian rotation period and the orbital period of the Phobos 2 spacecraft (~8 hours).

References and Notes

1. M. H. Acuña *et. al.*, *Science* **279**, 1676 (1998).
2. M. H. Acuña *et. al.*, *J. Geophys. Res.* **97**, 7799 (1992).
3. The Mars Global Surveyor magnetic field experiment provides fast (up to 32 samples per second) and precise (12-bit) vector measurements of the ambient field over the range of 4 to 65,536 nT per axis. It includes two fluxgate magnetometers mounted at the outer edge of the articulated solar panels and an electron reflectometer mounted on the spacecraft body that measures the local electron distribution function in the range of ~1 to 20 KeV to remotely sense the strength of magnetic fields of planetary origin at the top of the martian atmosphere. The observations reported here were acquired by the twin fluxgate magnetometer system.
4. The measurement error is determined primarily by incomplete knowledge of spacecraft-generated magnetic fields. These are associated with the electrical power system and uncompensated permanent magnets present in amplifiers mounted behind the spacecraft high gain antenna. During the cruise phase, spacecraft maneuvers in a fixed solar panel orientation were used to determine the instrument offsets to an estimated accuracy of 0.5 nT. In the aerobraking orbits, frequent spacecraft reconfigurations and articulations of the solar panels degrade the accuracy of the error estimate yielding the value quoted in the paper. The twin magnetometer configuration is used to identify spacecraft-generated magnetic fields and distinguish them from ambient field changes.
5. J. L. Le Mouël, V. Courtillot, J. Ducruix, *Geophys. J. R. Astron. Soc.* **42**, 251 (1975); J. Achache, A. Abdtout, J. L. Le Mouël, *J. Geophys. Res.* **92**, 11584 (1987); M. A. Mayhew, *ibid.* **45**, 119 (1975).
6. J. G. Luhmann and L. H. Brace, *Rev. Geophys.* **29**, 121 (1991).
7. D. E. Smith, private communication (1999).
8. The crater density shown overlaid with the magnetic field data in Fig. 3 has been adapted from the work of N. Barlow, *Encyclopedia of Planetary Sciences,* J. H. Shirley and R. W. Fainbridge, Eds. (Chapman & Hall, London, 1997), p. 454.
9. R. O. Pepin and M. H. Carr, in *Mars*, H. H. Kieffer *et al.*, Eds. (Univ. of Arizona Press, Tucson, 1992), pp. 120–143.
10. G. Schubert *et al.*, in (*9*), pp. 147–183; M. Leweling and T. Spohn, *Planet. Space Sci.* **45**, 11, 1389 (1997).
11. When a ferromagnetic material is heated above its Curie point, it loses all of its remanent magnetism and its ability to retain magnetism. Conversely, when a ferromagnetic material cools below its Curie point in the presence of an ambient magnetic field, it is able to retain a remanent field that provides information about the strength and direction of the original field in which it cooled. This is the process by which the martian crustal magnetic sources were formed.
12. D. E. Wilhelm and S. W. Squyres, *Nature* **309**, 138 (1984); H. V. Frey and R. A. Schultz, *Geophys. Res. Lett.* **15**, 229 (1988); G. E. McGill and A. M. Dimitriou, *J. Geophys. Res.* **95**, 12595 (1990).
13. J. G. Luhmann *et al.*, in *Mars*, H. H. Kieffer *et al.*, Eds. (Univ. of Arizona Press, Tucson, AZ 1992), pp. 1090–1134.
14. J. E. P. Connerney *et. al.*, *Science* **284**, 794 (1999).
15. D. Mohlmann *et al.*, *Planet. Space. Sci.* **39**, 83 (1991).
16. J. L. Inge and R. M. Batson, *U.S. Geol. Surv. Map 1322* (1982) (available at wwwflag.wr.usgs.gov/USGSFlag/Space/mapbook); E. Young, *Mars Atlas* (available at cmex.arc.nasa.gov/Atlas96/Atlas96.htm).

17. We thank the Mars Global Surveyor Project Office and the Mission Operations Team at JPL and Lockheed Martin Astronautics for the extraordinary efforts made to collect magnetic field data at periapsis during the second aerobraking phase. The contributions of D. W. Curtis, M. Kaelberer, D. Brain, F. Perin, and P. Lawton to the processing display and analysis of the magnetic field data are gratefully acknowledged. The research at UC Berkeley was supported by NASA grant NAG-5-959. N.F.N. acknowledges support in part by NASA grant NAG-5-3538.

15 March 1999; accepted 9 April 1999

Global Distribution of Crustal Magnetization Discovered by the Mars Global Surveyor MAG/ER Experiment

M. H. Acuña, J. E. P. Connerney, N. F. , Ness, R. P. Lin, D. Mitchell, C. W. Carlson, J. McFadden, K. A. Anderson, H. Rème, C. Mazelle, D. Vignes, P. Wasilewski and P. Cloutier

Science **284** (5415), 790-793.
DOI: 10.1126/science.284.5415.790